Three-Leaf Quantum Interference Clovers in a Trigonal Single-Molecule Magnet

Three-Leaf Quantum Interference Clovers in a Trigonal Single-Molecule Magnet

James H. Atkinson,[1] Ross Inglis,[2] Enrique del Barco,[1,*] and Euan K. Brechin[2]
[1]*Department of Physics, University of Central Florida, Orlando, Florida 32765, USA*
[2]*EaStCHEM School of Chemistry, The University of Edinburgh, West Mains Road, Edinburgh EH9 3JJ, United Kingdom*
(Received 7 May 2014)

We report on a single-molecule magnet where the spatial arrangement of three manganese ions and their spin-orbit coupling tensor orientations result in threefold angular modulations of the magnetization tunneling rates and quantum interference patterns that mimic the form of a three-leaf clover. Although expected in all quantum tunneling of magnetization resonances for a trigonal molecular symmetry, the threefold modulation only appears at resonances for which a longitudinal magnetic field is applied (i.e., resonance numbers $|k| > 0$). A sixfold transverse field modulation observed at a resonance of $k = 0$ manifests as a direct consequence of a threefold corrugation of the spin-orbit coupling energy landscape, creating an effective longitudinal field which varies the resonance condition in the presence of a transverse field. The observations allow for an association between the trigonal distortion of the local spin-orbit interactions and the spatial disposition of the constituent ions, a finding that can be extrapolated to other systems where spin-orbit coupling plays a significant role.

DOI: PACS numbers: 75.50.Xx, 03.65.Vf, 75.45.+j

One of the most prominent findings since the discovery of single-molecule magnets (SMMs) [1,2] is the significance of Berry phase interference (BPI) as a modulator of quantum tunneling of magnetization (QTM) [4–6], which established the importance of the subtle contributions of spin-orbit interactions in QTM behavior. It is in the kernel of this understanding where one finds insight into the relationship between the spin-orbit coupling (SOC) symmetries and QTM, including the symmetry-imposed spin selection rules. These rules state that in order for tunneling to occur between two spin eigenstates, labeled as m and m', at a QTM resonance $k = mn - m$, k must be an integer multiple of the lower molecular symmetry. As such, in molecules of rhombic symmetry, only resonances corresponding to a multiple of two are unfrozen, while trigonal and tetragonal symmetries only lift state degeneracies at resonances $k = 3 \times n$ and $k = 4 \times n$ (n = integer), respectively. These apparently clear restrictions have puzzled researchers in the field for two decades, as evidence for tunneling has been observed at all QTM resonances for most SMMs regardless of their respective molecular symmetry. The only exception so far has been a Mn_3 SMM of trigonal symmetry [13], in which the absence of a resonance ($k = 1$) provided the first clear evidence of spin selection rules. However, the appearance of other resonances also forbidden by symmetry (i.e., $k = 2$) in that molecule and the inability to study the detailed field dependence of the different tunnel splittings have dimmed the relevance of that finding, since its interpretation has relied exclusively upon theoretical analyses derived from indirect results (see Refs. [14–16]).

The lowest symmetry that supports QTM in odd-numbered resonances is trigonal. This is an important case study, as only a transverse magnetic field can break the degeneracy between the spin levels at odd-numbered resonances. It is worth noting that internal fields (e.g., dipolar or nuclear) are not sufficiently large enough to explain the observed tunneling rates in forbidden resonances. Thus far, the only indirect evidence of a trigonal molecular symmetry has been a sixfold magnetic field angular modulation of the electron paramagnetic resonance spectra in a heteronuclear Fe_3Cr SMM [16], while the corresponding modulation of the QTM remains unobserved for this symmetry. It is in this Letter where the first manifestation of a threefold modulation of the QTM rates in a SMM is presented. We also detail a number of related fascinating behaviors, including the first observation of a spatial corrugation of the intrinsic SOC energy landscape. The results presented here represent an important step forward in the effort to reconcile the theory of QTM with observation, and shed light on the answers of many long-standing questions.

The SMM complex we studied has the formula $Mn_3O(Et-sao)_3(Et-py)_3ClO_4$ (henceforth referred to as Mn_3). Chemical analysis [17] ascribes the magnetic behavior to a core containing three Mn^{III} ions ($s = 2$) ferromagnetically coupled via a superexchange interaction, resulting in an $S = 6$ ground state. A schematic constructed from x-ray diffraction measurements is inset in Fig. 1 (see Ref. [17] for more details).

Figure 1 shows magnetization hysteresis loops obtained from a crystalline sample of Mn_3 SMMs with a field applied along the easy anisotropy axis (z axis) at different temperatures. Note that resonance $k = 1$ does not appear below 1.35 K, due to the selection rules discussed above which forbid this resonance under trigonal symmetry

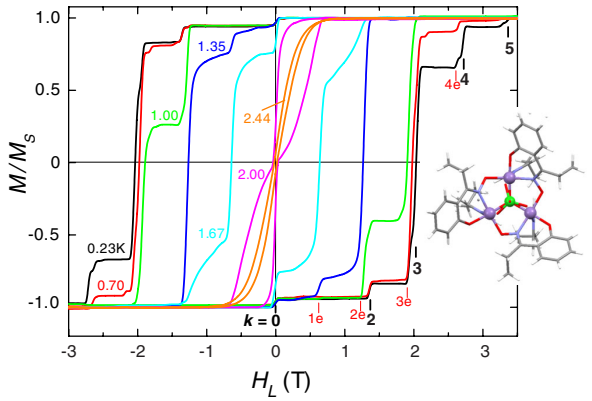

F1:1 FIG. 1 (color online). Stepwise magnetic hysteresis loops
F1:2 characteristic of resonant QTM obtained in a single crystal of
F1:3 $Mn_3O(Et-sao)_3(Et-py)_3ClO_4$ SMMs at different tempera-
F1:4 tures. Up to six resonances can be observed ($k = 0, \pm1, \pm2, \pm3,$
F1:5 ±4, and ±5), including steps associated with QTM through
F1:6 excited states ($k = 1e, 2e, 3e, n$). The inset shows the Mn_3 core.

considerations (i.e., $k \neq 3 \times n$). The QTM spectroscopy (i.e., position of the resonances) in this figure allows for determination of the spin Hamiltonian governing the sample's quantum dynamics. In the giant spin approximation (GSA), the molecule is considered as a single rigid spin (S) modeled by an interaction Hamiltonian, by which a trigonal symmetry can be written as follows:

$$\hat{H}_{\mathrm{GSA}} = D\hat{S}_z^2 + B\hat{S}_z^4 + B_4^3 O_4^3 + B_6^6 O_6^6 + \mu_B \boldsymbol{B} \cdot \overleftrightarrow{g} \cdot \hat{S}. \quad (1)$$

The first four terms characterize the zero-field splitting anisotropy, with the first usually dominant and responsible for the easy magnetization axis of the molecule (with a quartic axial correction given by the second). The Stevens spin operators (O_p^q) are restricted by the spin value ($p \leq 2S$) and the rotational symmetry, $q(\leq p)$. Here we consider only second-($\hat{S}_z^2 = O_2^0$, with $D = 3B_2^0$) and fourth-order ($B\hat{S}_z^4$) axial terms and the leading trigonal ($O_4^3 = \frac{1}{2}[\hat{S}_z, \hat{S}_+^3 + \hat{S}_-^3]$) and hexagonal ($O_6^6 = \frac{1}{2}[S_+^6 + \hat{S}_-^6]$) transverse operators. The final term is the spin-field Zeeman interaction. The QTM behavior in Fig. 1 can be well explained by diagonalization of the GSA Hamiltonian assuming an isotropic $g = 2$, $D = -0.86$ K, and $B = 1.4$ mK (the transverse anisotropy terms have a negligible effect on the spin projection energies, being only significant at degeneracies). Figure S1 in the Supplemental Material [19] shows the correspondence between the QTM spectroscopy data and the levels of the $S = 6$ spin multiplet.

We will focus the following discussion on the behavior of the QTM resonances as a function of both the angle and magnitude of the transverse field, H_T (see also Fig. S2 in the Supplemental Material [19] for a visualization of the molecular axes as defined by the molecular anisotropy). We define the QTM probability P_k as the normalized change in magnetization that occurs as the longitudinal field H_L is swept through a resonance. This probability is related to the "tunnel splitting" Δ_k (which breaks the degeneracy between opposite spin projections) by the Landau-Zener formula [18], $P_k = 1 - \exp[-\pi\Delta_k^2 n/2\upsilon_0\delta]$, where $\upsilon_0 = g\mu_B(2S-k)$, δ is the field sweep rate and n is the number of times resonance k is crossed. To extract the angular dependence of P_k, a fixed transverse field is maintained at a given angle ϕ within the molecular xy plane while the longitudinal field is swept across the resonance under study. The process is then repeated for different ϕ ranging from 0° to 360°. In order to optimize the quality of the results, and overcome several technical limitations, different protocols of measurement were followed for each resonance, as explained in Sec. 2 of the Supplemental Material [19].

Let us focus first on resonance $k = 0$. Figure 2(a) shows a polar plot of $P_{k=0}$ vs ϕ, where an extraordinary sixfold modulation emerges, with sharp minima occurring at angles $\varphi_{\mathrm{min},k=0}^{\mathrm{BPI}} = 32.6° + m \times 60°$ which correspond to BPI tunnel quenching. However, this sixfold appearance can be misleading; the expected symmetry of the molecule is threefold, and so the shape of the resonance behavior should be as well (in fact, we observe such modulation in all the other resonances, as discussed below). Within the GSA, this anomaly is a consequence of the trigonal transverse SOC anisotropy term, $O_4^3 = [\hat{S}_z, \hat{S}_+^3 \pm \hat{S}_-^3]$,

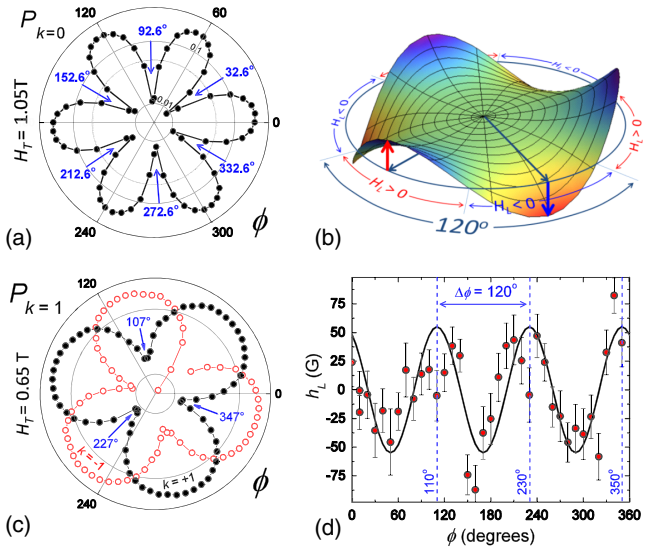

F2:1 FIG. 2 (color online). (a) Sixfold modulation of the QTM
F2:2 probability in resonance $k = 0$ as a function of the angle of a
F2:3 1.05 T transverse field in the molecular xy plane. Sharp minima
F2:4 appear every 60°. (b) Illustration of the threefold corrugation of
F2:5 the hard anisotropy plane which defines the longitudinal com-
F2:6 pensating field. (c) Data from our compensating field measure-
F2:7 ment (circles). The continuous line represents the fitting from
F2:8 diagonalization of the MS Hamiltonian in Eq. (2). (d) Threefold
F2:9 modulation of the QTM probability in resonances $k = \pm1$ as a
F2:10 function of the angle of a 0.65 T transverse field within the
F2:11 molecular xy plane, with sharp minima appearing every 120°.

which commutes the axial ($\hat{S}_z$) and the third-order creation or annihilation ($\hat{S}_+^3 \pm \hat{S}_-^3$) spin operators. Apart from generating a threefold modulation of the anisotropy barrier [see Fig. S2(b) in the Supplemental Material [19]], this term acts as an effective longitudinal field and produces a threefold corrugation of the hard anisotropy plane in the presence of transverse field, as illustrated in Fig. 2(b), and requires an offsetting or "compensating" longitudinal field (h_L) in order to bring the system back into resonance. This effect is extremely subtle and difficult to observe for the ground state splitting at resonance $k = 0$ (which mixes states $m = +6$ and $m' = -6$) in the range of H_T explored in these experiments, since the magnitude of h_L (<3 G) is much smaller than the effective field width of the resonance (~2000 G at $H_T = 1.2$ T). As explained in Sec. 2 of the Supplemental Material [19], a sophisticated measurement protocol was employed in order to discern the contribution of the compensating field, with measurements performed at higher temperature ($T = 1.57$ K) for which the $k = 0$ tunneling occurs predominantly through the third excited tunnel splitting (mixing states $m = +3$ and $m' = -3$). The corrugation is much more pronounced in this splitting as a result of its commensuration ($\Delta m = 3 \times n$) with the symmetry of the trigonal SOC term. The results are displayed in Fig. 2(c), where the compensating field shows an alternation between −55 and +55 Gauss with an overall threefold oscillation pattern. Interestingly, its absolute maximum values, found at $\varphi_{\max}^{|h_L|} = 50° + n \times 60°$, do not coincide with the angular positions of the BPI minima in this resonance ($\varphi_{\min,k=0}^{\mathrm{BPI}} = 32.6° + n \times 60°$), as would have been expected from Eq. (1).

The trigonal symmetry of this SMM becomes obvious in the resonances that require a nonzero longitudinal field, i.e., $|k| > 0$, and which produce clear threefold angular modulations of the QTM probabilities. Data for $k = \pm 1$ are shown in Fig. 2(d) (see Fig. S4 of the Supplemental Material [19] for $|k| > 1$). For positive longitudinal fields (solid black circles) minima are found at $\varphi_{\min,k>0}^{\mathrm{BPI}} = 107° + n \times 120°$, and correspond to conditions for destructive BPI. As a fascinating consequence of this symmetry, the anisotropy axes are "hard" and "medium" simultaneously, depending on the direction of both the longitudinal and transverse applied fields. If the longitudinal field is reversed, as in resonances $k < 0$ [open red circles in Figs. 2(d) and Fig. S4 [19]], the threefold modulation is shifted by 60°, with minima appearing at $\varphi_{\min,k<0}^{\mathrm{BPI}} = 47° + n \times 120°$, a consequence of the time-reversal invariance upon full reversal of the total magnetic field.

We now turn our attention to the modulation of the QTM as a function of the magnitude of the transverse magnetic field applied along the "hard-medium" axes within the molecular xy plane, i.e., $\varphi_{\min,k=0}^{\mathrm{BPI}} = 32.6°(+180°)$ for $k = 0$ and $\varphi_{\min,|k|>0}^{\mathrm{BPI}} = 107°(+180°)$ for $k > 0$. The results are shown in Fig. 3: $k = 0$ (solid black circles), $k > 0$ (solid red, green, and blue data points), and $k < 0$ (open data points). BPI minima are found near $H_{T,k=0}^{\mathrm{BPI}} = \pm 1.05$ T, $H_{T,k=\pm1}^{\mathrm{BPI}} = \pm 0.57$ T, $H_{T,k=\pm2}^{\mathrm{BPI}} = \pm 0.50$ T, and $H_{T,k=\pm3}^{\mathrm{BPI}} = \pm 0.35$ T (marked by arrows). These are the same transverse fields chosen for the angular modulation measurements in Figs. 2 and S4 (with the exception of $k = \pm 1$, in which a value of 0.65 T was used). The GSA Hamiltonian in Eq. (1) cannot account for the position of the BPI minima across all the resonances in Fig. 3 nor the difference in angles at which the BPI minima appear between resonances $k = 0$ [i.e., $32.6 + n \times 60°$, Fig. 2(a)] and $|k| > 0$ [$47° + n \times 60°$, Fig. 2(d)], with a relative shift of $\Delta\phi = 14.4°$. As mentioned above, a similar shift is also observed between the $k = 0$ BPI minima and the angles of the compensating field maxima [$\sim 50° + n \times 60°$, Fig. 2(c)], which also eludes explanation from Eq. (1). Interestingly, a 15° rotation of the trigonal O_4^3 with respect to the hexagonal O_6^6 transverse anisotropy term in Eq. (1) about the z axis can accurately account for all the observations (using $B_4^3 = -2.86 \times 10^{-4}$ and $B_6^6 = 11.46 \times 10^{-7}$ K), as shown in Fig. S6. Note that this rotation is equivalent to the inclusion of an imaginary O_4^{-3} term, as expected from the C_{3v} symmetry of the molecule, although it does not give information about its physical origin. A more natural approach, with real physical significance, is to employ a multispin interaction Hamiltonian which takes into account the constituent ions and the corresponding intramolecular interactions, as follows:

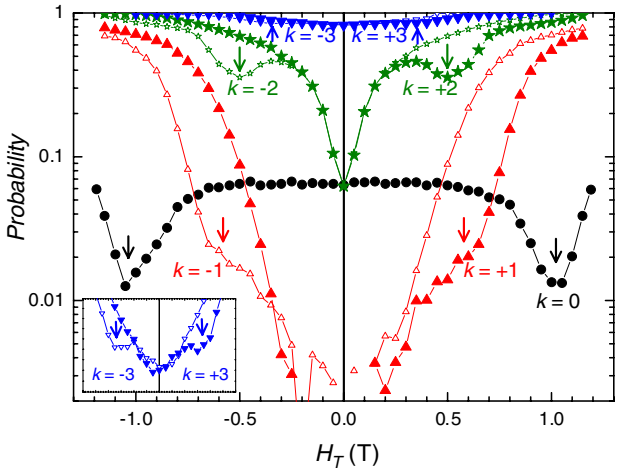

FIG. 3 (color online). QTM probability of resonances $|k| = 0$–3 as a function of transverse field applied along the axes at $\phi = 32.2°$ (+180°) for $k = 0$, and $\phi = 107°$ (+180°) for $|k| > 0$. Clear BPI minima are observed at $H_T = \pm 1.05$, ± 0.57, ± 0.50, and ± 0.35 T for resonances $k = 0$, ± 1, ± 2, and ± 3, respectively, as marked by the corresponding arrows. The inset shows a zoom to −0.6 to +0.6 T transverse field of the $k = \pm 3$ data. Reversal of the longitudinal field produces the specular image with respect to reversal of the transverse field, as imposed by the time-reversal invariance of the spin-orbit interaction.

$$\hat{H}_{\mathrm{MS}} = \sum_i \hat{s}_i \cdot \overleftrightarrow{R}_i^T \cdot \overleftrightarrow{d}_i \cdot \overleftrightarrow{R}_i \cdot \hat{s}_i + \sum_i g\mu_B \hat{s}_i \cdot \vec{B} + \sum_{i>j} \hat{s}_i \cdot \overleftrightarrow{J}_{i,j} \cdot \hat{s}_j, \quad (2)$$

where $\hat{s}_i$ is the spin operator of the ith ion, $\overleftrightarrow{d}_i$ is a diagonal 3×3 matrix with values e_i, $-e_i$, and d_i (representing the rhombic and axial anisotropy terms of the ith ion), and $\overleftrightarrow{J}_{i,j}$ is the exchange coupling tensor between each pair (i, j) of spins. This model not only permits consideration of the couplings between the spins of the constituent ions (therefore explaining the presence of excited spin multiplets and accounting for all the observed QTM steps; see Fig. S1 in the Supplemental Material [19]), but also allows for an arbitrary rotation of the single-ion SOC tensors, achieved by the matrix $\overleftrightarrow{R}_i^T$ and characterized by the Euler angles α_i, β_i, and γ_i, as illustrated in Fig. 4.

The angles α_i and γ_i are identical for all ions (i.e., become simply α and γ), while β_i are spaced by 120°, as imposed by the molecular symmetry. All angles are unambiguously determined by the particulars of the BPI behavior within the transverse field magnitude-angle phase space (demonstrating the importance of observing the BPI). Our simulations indicate that varying α has a strong effect on the magnitudes of transverse field at which the minima occur for resonances $k = 1, 2, 3$. This dependence is shown in Fig. 4(a) as obtained from diagonalization of Eq. (2) using the following parameters: $g_i = 2$, $d = -3.6$ K, $e = 0.62$ K, isotropic $J = 3.1$ K, $\beta_1 = 0°$, $\beta_2 = 120°$, and $\beta_3 = 240°$. Note that $k = 0$ remains unaffected for small values of α, which is no surprise as this resonance is the only one allowed in the absence of any local ion tilts. The positions at which we experimentally observe the minima are indicated in Fig. 4(a), and coincide with predicted values for a tilt of $\alpha = 6°$. The value of γ generates an angular phase shift ($\Delta\phi$) between the modulation of the BPI in $k = 0$ and the other resonances, as shown in Fig. 4(b). The experimentally observed value for this shift is $\Delta\phi_{\mathrm{exp}} = 14.5°$, which agrees with the calculated difference for an angle of $\gamma = 33°$ ($\Delta\phi_{\mathrm{th}} = 14.4°$). This set of angles explains all the novel experimental findings provided in this Letter, producing the BPI patterns displayed in Figs. S4 and S6 [19], including the fitting of the compensating longitudinal field in Fig. 2(c) (see the Supplemental Material [19] for details of the fitting).

An important aspect which is experimentally observed for the first time in these results is the difference between the transverse field dependencies of the $k = 1$ and $k = 2$ resonance splittings, with $\Delta_{k=1}$ growing much more slowly than $\Delta_{k=2}$ with increasing transverse field (Fig. 3). This is crucial in understanding the appearance of one of the two forbidden resonances, as the sole contribution of small internal transverse fields (dipole or hyperfine fields) can unfreeze QTM in resonance $k = 2$, while much larger field values would be necessary to similarly affect resonance $k = 1$. Together with the effect of local disorder-induced distortions (as discussed in Ref. [15]), this result may explain why QTM is observed at all resonances in most SMMs regardless of the selection rules imposed by the SOC symmetry.

Finally, the precision in the association of the MS Hamiltonian terms with the observed phenomena allows determination of the single-ion anisotropy tensors in relation to the specifics of the chemical arrangement with an unprecedented degree of accuracy, as we show in Sec. 5

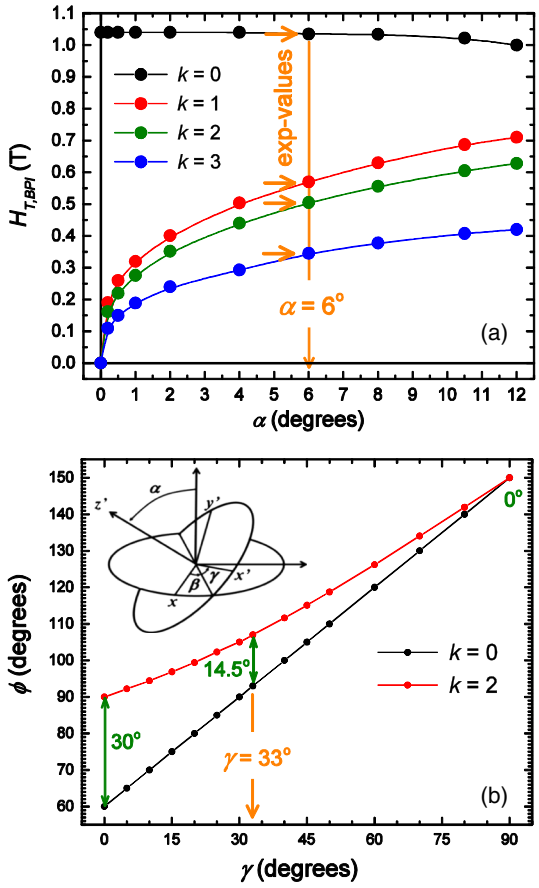

FIG. 4 (color online). (a) Transverse field positions of the BPI minima for resonances $k = 0$–3 as a function of the Euler angle α, which represents the tilt of the ion easy axis away from the overall molecular easy z axis. The arrows indicate the values observed experimentally (see Fig. 3), which coincide for an angle of $\alpha = 6°$. (b) Calculated angular positions of the BPI minima in resonances $k = 0$ and $k = 2$ as a function of the rotation Euler angle γ. The observed angular shift of $\Delta\phi_{\mathrm{exp}} = 14.5°$ is theoretically matched with a value of $\gamma = 33°$. The inset illustrates an arbitrary α-β-γ Euler rotation of the second-order SOC tensor of a single manganese ion. The vector from the center of the triangle formed by the three ions to the first ion is approximately equivalent to the $\phi = 0$ (within the $\pm 3°$ uncertainty in the exact position of the crystal in our sensor), which is coincident with the $\beta_1 = 0$ axis.

of the Supplemental Material [19]. The magnetization studies presented here show a clear correlation between the chemical structure and the form of the SOC anisotropy or energy landscape of the spin of a SMM, and represent a nearly full treatment of QTM phenomenon. By illustrating the potential for such high-resolution examinations of the molecular symmetry, we see a vast and rich frontier remaining to be explored by the pairing of molecular engineering and low temperature physics experiment.

J. H. A. and E. d. B. acknowledge support from the National Science Foundation (Grant No. DMR 0747587). E. K. B. thanks EPSRC for funding.

*To whom correspondence should be addressed.
delbarco@physics.ucf.edu

[1] Sessoli R, D. Gatteschi, A. Caneschi, and M. A. Novak, Nature (London) **365**, 141 (1993).
[2] J. R. Friedman, M. P. Sarachik, J. Tejada, and R. Ziolo, Phys. Rev. Lett. **76**, 3830 (1996).
[3] L. Thomas, F. Lionti, R. Ballou, D. Gatteschi, R. Sessoli, and B. Barbara, Nature (London) **383**, 145 (1996).
[4] D. Loss, D. P. DiVincenzo, and G. Grinstein, Phys. Rev. Lett. **69**, 3232 (1992).
[5] J. von Delft and C. L. Henley, Phys. Rev. Lett. **69**, 3236 (1992).
[6] A. Garg, Europhys. Lett. **22**, 205 (1993).
[7] W. Wernsdorfer and R. Sessoli, Science **284**, 133 (1999).
[8] E. del Barco, A. D. Kent, E. M. Rumberger, D. N. Hendrickson, and G. Christou, Phys. Rev. Lett. **91**, 047203 (2003).
[9] S. T. Adams, E. da Silva Neto, S. Datta, J. Ware, C. Lampropoulos, G. Christou, Y. Myaesoedov, E. Zeldov, and J. Friedman, Phys. Rev. Lett. **110**, 087205 (2013).
[10] C. M. Ramsey, E. del Barco, S. Hill, S. J. Shah, C. C. Beedle, and D. N. Hendrickson, Nat. Phys. **4**, 277 (2008).
[11] H. M. Quddusi, J. Liu, S. Singh, K. J. Heroux, E. del Barco, S. Hill, and D. N. Hendrickson, Phys. Rev. Lett. **106**, 227201 (2011).
[12] J. J. Henderson, C. Koo, P. Feng, E. del Barco, S. Hill, I. Tupitsyn, P. Stamp, and D. Hendrickson, Phys. Rev. Lett. **103**, 017202 (2009).
[13] J. Liu, E. del Barco, and S. Hill, Phys. Rev. B **85**, 012406 (2012).
[14] J. Liu, E. del Barco, and S. Hill, *Molecular Magnets: Physics and Applications*, edited by J. Bartolome, F. Luis, and J. F. Fernandez (Springer, New York, 2013).
[15] L. Sorace, M.-E. Boulon, P. Totaro, A. Cornia, J. Fernandes-Soares, and R. Sessoli, Phys. Rev. B **88**, 104407 (2013).
[16] R. Inglis, S. M. Taylor, L. F. Jones, G. S. Papaefstathiou, S. P. Perlepes, S. Datta, S. Hill, W. Wernsdorfer, and E. K. Brechin, Dalton Trans. 9157 (2009).
[17] P. L. Feng, C. Koo, J. J. Henderson, M. Nakano, S. Hill, E. del Barco, and D. N. Hendrickson, Inorg. Chem. **47**, 8610 (2008).
[18] C. Zener, Proc. R. Soc. A **137**, 696 (1932).
[19] See the Supplemental Material at http://link.aps.org/supplemental/10.1103/PhysRevLett.000.000000 for details.